Department of Veterans Affairs

Journal of Rehabilitation Research and Development Vol. 35 No. 1, January 1998
Pages 61–72

Three-dimensional kinematics of the shoulder complex during wheelchair propulsion: A technical report

Jaime L. Davis, BA; Eric S. Growney, BS; Marjorie E. Johnson, MS, PT; Brian A. Iuliano, BS; Kai-Nan An, PhD
Orthopedic Biomechanics Laboratory, Mayo Clinic/Mayo Foundation, Rochester, MN 55905

Abstract—Methods for the three-dimensional (3-D) kinematic analysis of the shoulder complex (humerus relative to trunk) are presented and their use demonstrated in this analysis of shoulder motion during wheelchair propulsion. Ten subjects propelled two different wheelchairs (adjustable and conventional chairs) while the motions of the left arm and trunk were measured using a video tracking system. Eulerian angles described the sequence-dependent rotations of the humerus relative to the trunk. Wheel angular velocity and acceleration, hand position on the handrim, and duration of cycle subphases were also measured. Selected temporal and kinematic parameters were derived from the time-normalized average cycle of each subject on each wheelchair. Within-subject variation of these parameters according to wheelchair type were compared using a two-tailed t-test for paired observations.

The adjustable chair made available a larger propulsion arc compared with the conventional chair. Only the minimum amount of elevation demonstrated a significant difference between chairs (the conventional chair had a smaller minimum than the adjustable chair) at the corrected significance level of $p<0.001$. Other differences, though not statistically significant, were still informative. Less shoulder internal rotation but more overall shoulder motion was observed during recovery phase in the adjustable chair as compared with the conventional chair. The methods presented for measuring the 3-D kinematics of the shoulder complex during wheelchair propulsion proved feasible for future use in studies that will address shoulder kinetics, energy requirements, wheelchair design, and chronic use disorders.

This material is based upon work supported by the Mayo Foundation, Rochester, MN.

Address all correspondence and requests for reprints to: Kai-Nan An, PhD, Orthopedic Biomechanics Laboratory, Mayo Clinic/Mayo Foundation, Rochester, MN 55905; email: an@mayo.edu.

Key words: *Euler angles, shoulder, wheelchair.*

INTRODUCTION

An estimated 1.2 million Americans use wheelchairs as their primary means of mobility (1,2). As a result, wheelchairs have become commonplace in society while improving the functional independence of those with disabilities. Despite the prevalence of wheelchair use and associated upper limb injuries, wheelchair propulsion biomechanics have been a subject of relatively recent investigation. Early shoulder-related studies date back only to the 1970s (1–6). In 1979, Nichols et al. (5), studied the incidence of upper limb pain among 491 "spinally paralyzed" members of the British Spinal Cord Injuries Association and found a 51.4 percent incidence of shoulder pain, a higher incidence rate than in any age-matched control group. Bayley et al. (1) in 1987, found a 31 percent prevalence of chronic shoulder problems, of which the most common was chronic rotator cuff impingement syndrome with subacromial bursitis. The authors suggested that the shoulder motion during propulsion contributed to this high rate of impingement. Several authors have shown that the incidence of shoulder complaints increases with duration of disability, hence duration of wheelchair use (3–5). Gellman, Sie, and Waters (4) found that the most common complaint (30 percent) of the 84 persons with paraplegia they studied was shoulder pain. Corcoran et al. (7) and Ferrara and Davis (8) have emphasized the enhanced risk for injury of the

shoulder in elite wheelchair athletes. Pentland et al. (2) included an examination of upper limb pain in 11 women with long-term paraplegia, and found that 63 percent of subjects experienced shoulder pain during outdoor wheeling. These studies confirm the high incidence of shoulder pain associated with long-term wheelchair use seen in persons of both genders with paraplegia.

Few studies have analyzed wheelchair propulsion as compared with other locomotion. One reason for this is that the upper limb is not typically associated with mobility as is the lower, though this association is changing. Additionally, the techniques for studying the lower limb are well established, while those for the upper are in earlier stages of development. Even fewer studies have utilized a full, three-dimensional (3-D) description of the upper limb kinematics or kinetics involved with wheelchair propulsion because of the increased complexity and error sensitivity of these descriptions compared with two-dimensional (2-D), sagittal plane-only descriptions. However, 3-D studies are especially relevant because out-of-plane motion, like shoulder abduction and rotation, may contribute to musculoskeletal overuse injuries.

Numerous studies have examined wheelchair propulsion from a physiologic standpoint (7,9–30). However, until the recent interest in sports for the physically challenged, studies describing biomechanical and kinesiologic parameters of wheelchair use (25,26,31–41) were rare. Even fewer directly compare wheelchair designs (20,42).

An investigation of wheelchair biomechanics performed by Cerquiglini et al. (33) studied the kinematic, kinetic, and electromyographic patterns during wheelchair propulsion in a modified conventional chair on a variable incline ergometer. Sanderson and Sommer (36) performed a 2-D (sagittal plane) kinematic analysis of shoulder and elbow joint kinematics on three athletes with paraplegia propelling a conventional style wheelchair, using high-speed cinematography to compare propulsion styles. Van Der Woude et al. (26) examined the effect of seat height on the physiology, gross mechanical efficiency, and upper arm kinematics in nine control males propelling a basketball chair on a motor-driven treadmill. They observed a relationship between wheelchair seat height and both cardiorespiratory and kinematic parameters. These results were supported in a more recent study by Masse et al. (35) who found lower seat positions produced smoother upper limb motions.

Although not an exhaustive review, these studies are indicative of the current state of understanding of wheelchair propulsion and suggest that certain wheelchair parameters, including seat height and wheel camber, need to be considered (if not standardized) with respect to the size and gender of study participants. The predominance of 2-D kinematic studies that only examine sagittal plane motion also supports the need for full 3-D analyses of this complex problem.

The purpose of this study was to document and demonstrate a technique that uses a video tracking system for measuring the 3-D kinematics of the shoulder complex during wheelchair propulsion. Although it is recognized that such motion involves the intricate linkages between the humerus, scapula, and thorax, kinematic distinctions between these rigid bodies were not considered in this protocol, and instead, only the gross motion of the humerus relative to the trunk was considered. As a preliminary and demonstrative application of this kinematic measurement technique, the effect of wheelchair design (independent variable) on the temporal and 3-D kinematic parameters (dependent variables) of the shoulder complex during wheelchair propulsion were investigated. This is intended to be an initial step toward more comprehensive studies of wheelchair biomechanics.

METHODS

Subjects

The left upper limbs of 10 males who were minimally experienced in wheelchair propulsion and had no history of musculoskeletal or cardiorespiratory pathology were subjects for this study. The height, weight, arm length (acromion to tip of third digit), and trunk length (acromion to seat base) were measured on each subject. These data are presented in **Table 1.**

Table 1.
Subject anthropometries.

	Age	Weight	Height	Arm Length	Trunk Length
Mean	28.1	80.3	182.8	81.3	61.6
SD	1.4	2.3	1.8	1.0	0.9
Maximum	36	88.5	193.0	86.5	67.0
Minimum	25	69.4	175.0	77.0	56.0

Age in years, weight in kg, height and lengths in cm.

Although experienced wheelchair users with disabilities have been shown to be more efficient in the wheelchair propulsion task (32,38) and to differ in the biomechanics of the task (17,28,29,32,34,43–45), there were several practical reasons for selecting a group of controls. First, since one of the goals of this study was to test an upper limb measurement protocol, it was most practical to test it on nonimpaired subjects first, since they were easier to recruit and call back for repeat measurements if necessary. In addition, a control group reduced the variability that would be introduced by a study group with differences in level and completeness of neurologic injury. Although a study that included these differences may bring an important understanding to the demands of the wheelchair propulsion task on the typical user, it was important to eliminate that variable in this verification study. However, once verified, this protocol and kinematic model can be used for investigating such issues in ordinary wheelchair propulsion. Finally, since this study compared two wheelchairs commonly chosen as the first chair prescribed to a new user, inexperienced controls were considered an appropriate paradigm for a new user of a wheelchair.

Equipment

Subjects propelled each of two wheelchairs, in random order, on a wheelchair roller system (46). Despite the inhibition of independent control of the wheels as occurs during unconstrained wheelchair propulsion, straight-ahead propulsion is a symmetrical activity (41) that was safely and accurately simulated on this device. Prior to data collection, subjects were given basic instructions in the commonly used circular technique of wheelchair propulsion (36,38), wherein the hand follows a somewhat elliptical trajectory in the sagittal plane. The testing began with a 1-second static position data collection to define the wheelchair coordinate system. Motion data were collected to obtain five propulsion cycles (handrim contact to handrim contact). The static and motion data collections were then repeated for the second wheelchair.

The wheelchairs used were the 'Traveler' (Everest & Jennings, Inc., Camarillo, CA), a conventional, nonadjustable chair, and the 'Quickie 2' (Sunrise Medical, Fresno, CA), a lightweight, adjustable chair. The Quickie 2 (Q2) was adjusted to a commonly prescribed standard configuration of 0° wheel camber (exactly vertical), maximum rearward axle position, and axle plate height at one setting above minimum. This configuration placed the rear wheel axle 2.5 cm in front of the back edge of the seat. For the Traveler (T) chair, the 0° wheel camber, seat height, and rear axle position as far back as the rear edge of the seat were set by the manufacturer and cannot be adjusted. The same standard foam seat cushion was used with each chair, placing the user 17.8 cm above the rear wheel axle for both chairs. The wheel diameter was 61 cm for Q2 and 58.5 cm for T. This placed the wheelchair user 1.25 cm higher above ground and put the top of the wheel 1.25 cm higher above the seat in Q2 compared with the T. The T arm rests were 22.9 cm above the seat, while the Q2 arm rests were 36.8 cm above the seat. The standard pneumatic tires on the Q2 were kept inflated to manufacturer's recommendations.

A four-camera Expert Vision™ video-tracking system (Motion Analysis Corporation, Santa Rosa, CA) was used to capture 3-D trajectories of markers placed on the left upper limb, trunk, and wheelchair (**Figure 1**) at a rate of 60 frames/s. Prior to kinematic modeling, the video marker trajectories were run through a second-order Butterworth filter that implemented time

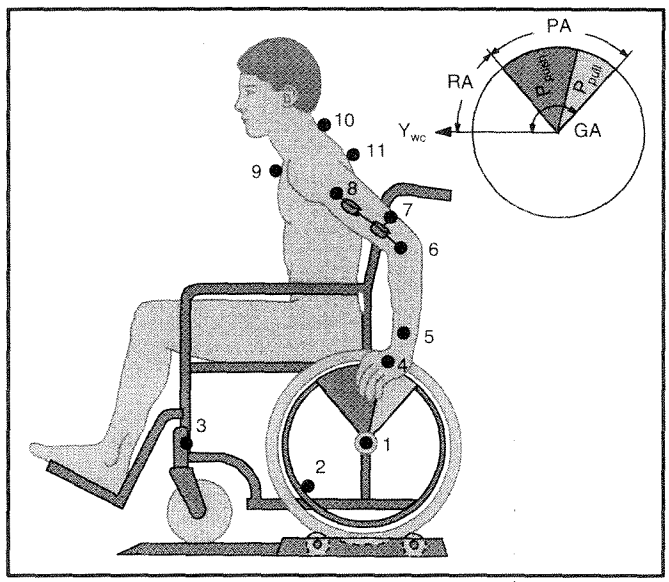

Figure 1.
Marker placement sites: 1) rear wheel axle; 2) periphery of spoke near hand rim; 3) front wheel post; 4) left mid-point third metacarpal; 5) 4 cm proximal to left mid-interstyloid line; 6) over left lateral epicondyle of humerus; 7) over left lateral supracondylar ridge of humerus; 8) just proximal to deltoid tuberosity of left humerus; 9) manubrium of sternum; 10) spinous process of C7; and 11) spinous process of T6. The inset illustrates the definitions of the Grab Angle (GA), Release Angle (RA), Propulsion Arc (PA), and the arcs during the pull and push phases of propulsion (Ppull and Ppush).

Journal of Rehabilitation Research and Development Vol. 35 No. 1 1998

reversal to avoid nonlinear phase shifts; the filter was set to a cutoff frequency of 6 Hz.

Kinematic Modeling

The Wheelchair Coordinate System (WCS) was determined using the static and motion trials. During each motion data collection, the time series circular trajectory of the rim marker (Marker 2 in **Figure 1**) was used in a Principle Component Analysis (47) to determine the unit vector perpendicular to the plane of the wheel (the Eigenvector of the coordinate covariance matrix having the greatest Eigenvalue) and was made the WCS z axis. A second vertical unit vector, x′, was formed from the static data collection of the corresponding wheelchair so that it pointed from the wheel center marker (Marker 1 in **Figure 1**) to the rim marker positioned at the "twelve o'clock," or vertical position on the wheel. A vector cross product between the z and x′ axes formed the WCS y axis. The true WCS x axis was then formed from the cross product of y and z axes. These unit vectors were the basis for the WCS, with the origin at the wheel center marker. All marker coordinates and subsequent kinematic descriptions were then expressed with respect to the WCS.

The wheel angle was calculated by the dot product between the WCS y axis and unit vector pointing from the wheel center marker to rim marker positions during the motion trials. Angular velocities and accelerations were determined using the GCVSPL algorithm (48) for differentiation of the wheel angle by approximating the wheel angle time series data with a quintic spline. The hand marker allowed for calculation of "grab angle" (GA), "release angle" (RA), "propulsion arc" (PA=RA−GA), the pull arc, and the push arc (**Figure 1,** inset). The GA was found by vector dot product between the WCS y axis and the vector connecting the wheel center marker to the hand marker (Marker 4, **Figure 2**) at the time of grab. The RA was similarly determined, but found at the time of release. For the purposes of this study, initial hand contact, or grab, was defined to be the time at which transition occurs from negative to positive wheel angular acceleration and release was the time of transition from positive to negative wheel angular acceleration.

The Trunk Coordinate System (TCS) was formed using the 3-D trajectories of markers placed at C7, T6, and the manubrium of the sternum (**Figure 1**) during the motion trials. The TCS z axis was formed as the unit vector pointing from the T6 marker to the sternum marker. A vector cross product between the TCS z axis and a unit vector pointing from the marker at T6 to the marker at C7 provided the left-pointing TCS y axis, enabling the formation of the TCS x axis.

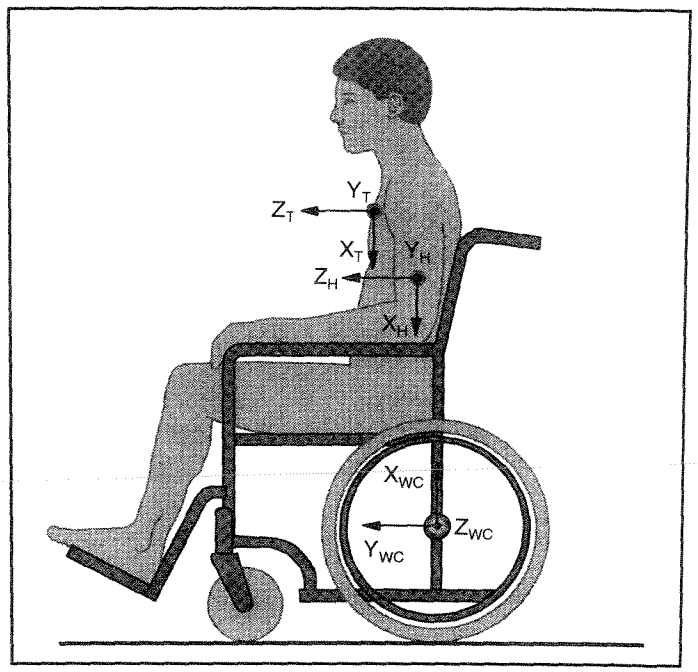

Figure 2.
The wheelchair coordinate system (WCS), trunk coordinate system (TCS), and humeral coordinate system (HCS) axes derived from marker positions.

The Humerus Coordinate System (HCS) was formed using the trajectories of three non-collinear markers rigidly fixed to a double pedestal "pod." This pod was secured to the skin over the deltoid tuberosity and the distal lateral supracondylar ridge of the left humerus so that one of the markers overlaid the lateral epicondyle (**Figure 1**). The HCS x axis was the unit vector pointing from the deltoid tuberosity pod marker to the lateral epicondyle pod marker. A vector cross product between this HCS x axis and a unit vector pointing from the deltoid tuberosity to the most lateral pod marker (Marker 7, **Figure 1**) formed the HCS z axis, subsequently enabling the HCS y axis formation. The WCS, TCS, and HCS are shown in **Figure 2.**

A sequence-dependent Euler angle set (**Figure 3**) was used to represent the motion of the HCS with respect to the TCS (49). The first humeral rotation from the anatomic neutral position was considered to be about the HCS x axis (parallel to the TCS x axis in the anatomic position) by an amount ϕ, describing the plane

of arm elevation. Thus, internal rotation from neutral would be modeled as a positive angle ϕ, and external rotation would be modeled as a negative angle. The humerus then rotated about the HCS z′ axis (HCS z in its new position) by an amount θ, to describe the amount of arm elevation. As such, an "abduction" or motion of the humerus away from the trunk would be modeled as a positive angle θ. Finally, the humerus was considered to be rotated axially about the HCS x″ axis (HCS x in its new position), by an amount ψ, to describe arm orientation with positive angle ψ for internal rotation and negative ψ for external rotation. The transformation matrix describing the distal HCS with respect to the proximal TCS was performed (50) as follows:

$$\begin{vmatrix} X\cdot x & X\cdot y & X\cdot z \\ Y\cdot x & Y\cdot y & Y\cdot z \\ Z\cdot x & Z\cdot y & Z\cdot z \end{vmatrix} =$$

$$\begin{vmatrix} c(\theta) & -c(\psi)s(\theta) & s(\psi)s(\theta) \\ s(\theta)c(\phi) & \begin{matrix} c(\psi)c(\theta)c(\phi) \\ -s(\psi)s(\theta) \end{matrix} & \begin{matrix} -s(\psi)c(\theta)c(\phi) \\ -c(\psi)s(\phi) \end{matrix} \\ s(\theta)s(\phi) & \begin{matrix} c(\psi)c(\theta)s(\phi) \\ +s(\psi)c(\phi) \end{matrix} & \begin{matrix} -s(\psi)c(\theta)s(\phi) \\ +c(\psi)c(\phi) \end{matrix} \end{vmatrix}$$

where s=sine and c=cosine. The x, y, and z represent the HCS unit vectors, and X, Y, and Z represent the corresponding TCS unit vectors, and all were expressed in the WCS. The three Eulerian angles could then be calculated from this matrix as follows:

$$\theta = \cos^{-1}(X \cdot x)$$
$$\phi = \cos^{-1}[(Y \cdot x)/\sin(\theta)] = \sin^{-1}[(Z \cdot x)/\sin(\theta)]$$
$$\psi = \cos^{-1}[-(X \cdot y)/\sin(\theta)] = \sin^{-1}[(X \cdot z)/\sin(\theta)]$$

This represents the "cyclic" 1–3′–1″ rotation sequence, or an x–z′–x″ sequence. In the neutral position, the HCS and TCS are assumed to be parallel and subsequently measure zero rotation. All rotations were measured in degrees and represent the kinematics of the shoulder complex at large.

Euler angles measuring trunk orientation relative to the WCS were similarly determined directly from the TCS matrix. However, in the interest of maintaining focus, those results were not explicitly documented in this report. These data were used subjectively in the discussion of the shoulder kinematic results. The elbow flexion angle was calculated using a vector dot product between the HCS x axis and a unit vector pointing along the forearm from the lateral epicondyle marker to the wrist marker (Marker 5, **Figure 2**). These data were not explicitly reported, but used in the data reduction process.

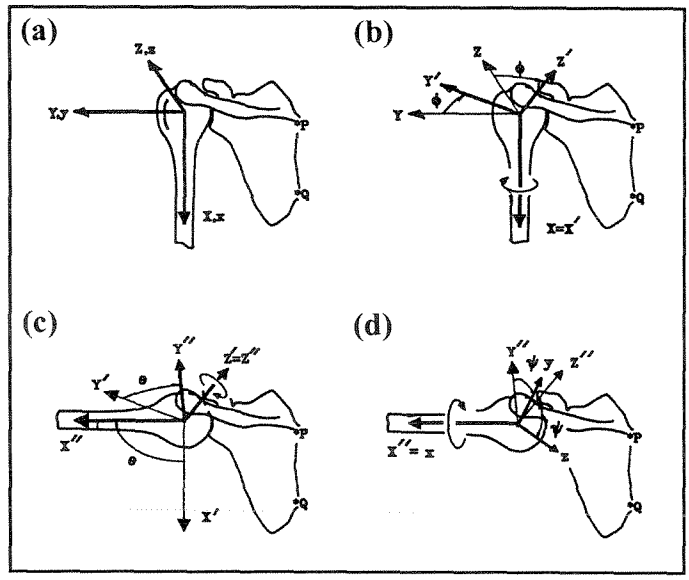

Figure 3.
Definition of the 1–3′–1″ rotation sequence. a) Starting from the anatomic neutral position. b) The first humeral rotation from the anatomic neutral position is about the HCS x axis (parallel to the TCS x axis in the anatomic position) by an amount ϕ, describing the plane of arm elevation. c) The humerus is then rotated about the HCS z′ axis (HCS z in its new position) by an amount θ, to describe the amount of arm elevation. d) The third and final angle is considered to be a rotation axially about the HCS x″ axis (HCS x in its new position), by an amount ψ, to describe arm orientation.

Data Reduction and Statistical Analysis

The wheelchair propulsion cycle was divided into two main phases: a propulsion phase (PP), during which the hands were in contact with the handrims and exerting force, and a recovery phase (RP), during which the hands were being repositioned for the next PP. The PP was determined and defined as the period during which a positive wheel angular acceleration occurred, while RP was that portion of the cycle during which a negative wheel angular acceleration occurred. Peak elbow flexion angle during hand contact was used to determine the transition between the 'pull' and 'push' sub-phases of the main PP, that for the purposes of this

Table 2.
Comparison of temporal parameters.

	Wheelchair Type							
	Q2		T		Difference		P Value	
Parameter	s	%	s	%	s	%	s	%
Propulsion								
Time (PT)	0.42	40.4	0.37	37.5	0.05	2.9	0.0167	0.0998
Pull time	0.28	26.9	0.21	21.1	0.07	5.8	0.0121	0.0295
Push time	0.14	13.5	0.16	16.4	0.02	2.9	0.3800	0.1270
Recovery								
Time (RT)	0.62	59.6	0.61	62.5	0.01	2.9	0.7102	0.0998
Total Cycle	1.04	100.0	0.98	100.0	0.06	—	0.0099	—
PT/RT Ratio	0.68		0.61					

s = seconds (absolute times); % = percentage of total cycle time (relative scale).

study were identified as 'Ppull' and 'Ppush', respectively (see **Figure 1**).

The data from five complete propulsion cycles for each subject in each wheelchair were time-normalized with quintic spline interpolation using the GCVSPL algorithm (48). The time-normalized data curves were then used to compute within-subject averaged cycle curves for each wheelchair. These time-normalized averages were then averaged across all subjects to yield a grand ensemble averaged cycle curve for each wheelchair.

Selected temporal and kinematic parameters (dependent variables) were derived from each subject's time-normalized average cycle data for each wheelchair (independent variable). Within-subject variation of these parameters due to wheelchair type were compared using a two-tailed t-test for paired observations (N=10), since only two treatment conditions were used. To reduce the chance of experimental error, the Bonferroni correction for multiple comparisons was applied. The pre-correction significance level of $p<0.05$ was chosen for all comparisons. After correcting the significance level and accounting for a two-tailed test as calculated by 0.05/(2×26 independent tests), the new significance level was determined to be $p<0.001$. The exact p values for all t-tests performed are shown so that the reader can interpret this information in light of the more stringent corrected significance level (51).

The temporal parameters selected for analysis were measured on absolute (seconds) and relative scales (percent of total cycle time). The parameters selected were total propulsion time (PT), that included the durations of Ppull and Ppush sub-phases, recovery time (RT), total cycle time (CT), and the propulsion time to cycle time (PT/CT) ratio. The kinematic parameters selected for statistical analysis were the handrim angular displacements, such as GA, RA, PA, the pull arc, and the push arc. The humeral angular displacements of ϕ (plane of elevation), θ (amount of elevation), and ψ (internal-external rotation) were also evaluated at these specific points in the propulsion cycle: the time at grab, the time at the changeover from Ppull to Ppush, the time at release, and the times and percent of cycle where maximum and minimum values were reached for each angle.

RESULTS

Temporal Parameters

The temporal parameter values, differences between chairs, and their p values are presented in **Table 2.** At the corrected significance level of $p<0.001$ none of these differences were considered to be significant.

Numerical values of the handrim contact angles, the differences between chairs, and their p values are presented in **Table 3.** The GA took place behind the "twelve o'clock" position (the WCS x axis) on the wheel in both chairs, an average of 32.41° in Q2 and of 23.07° in T: a significant difference at the $p<0.001$ level ($p=0.0002$) of nearly 10°. The changeover from Ppull to Ppush took place 4.04° behind the "twelve o'clock" wheel position in Q2 and 1.06° in front of it in T. These values are also significantly different. The average cycle

Table 3.
Comparison of handrim angular displacements.

Parameter	Wheelchair Type Q2 °	Q2 %	T °	T %	Difference °	Difference %	P Value °	P Value %
Grab Angle	122.41	—	113.07	—	9.34	—	0.0002	—
Pull Arc	28.37	26.9	24.13	21.1	4.24	5.8	0.0430	0.0295
Angle at Δ Ppull to Ppush	94.04	26.9	88.94	21.1	5.10	5.8	0.0005	0.0295
Push Arc	33.82	13.5	33.01	16.4	0.73	2.9	0.7341	0.1265
Release Angle	60.22	40.4	55.85	37.5	4.37	2.9	0.0557	0.0998
Propulsion Arc	62.19	40.4	57.22	37.5	4.96	2.9	0.0300	0.0998

° = degrees of arc displacement (absolute displacement); % = percentage of total cycle at which the displacement was measured.

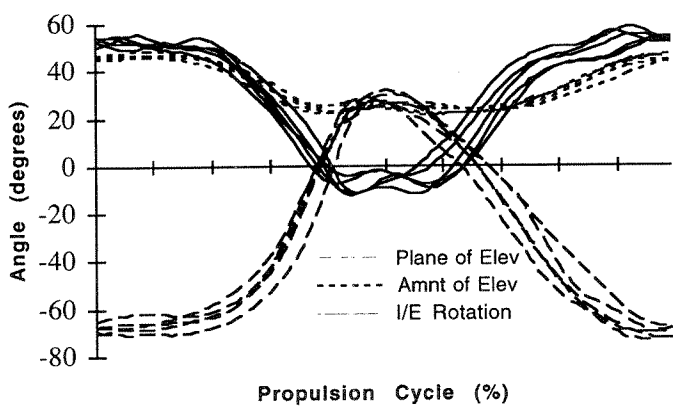

Figure 4.
Shoulder angles for five complete cycles from one randomly selected subject. The observable reproducibility was representative of all subjects.

time for the Q2 was longer than that for chair T, but the difference was not statistically significant (p=0.0099).

Shoulder Complex Kinematics

Between cycle reproducibility for one randomly selected subject is illustrated in **Figure 4.** This graph shows superimposed, time-normalized, humeral angular displacement curves for each of the representative subject's five complete cycles in one chair. **Table 4** lists the numerical values of the humeral angular displacements selected for statistical analysis using the paired t-test. The differences between chairs and the p values of the differences are shown as well.

Maximal plane of elevation (**Figure 5**) took place shortly after release in both chairs, and the minimum plane of elevation angle was seen just after grab. These angle differences were not shown to be statistically significant between chairs. Maximal plane of elevation in chair Q2 tended to occur slightly later in the cycle than it did in T, though this difference was not significant. During Ppull in the Q2, a plateau in the amount of elevation angle was observed (**Figure 6**). The amount of elevation decreases during the final portion of the PP. During the RP, the minimum angles were significantly less in chair T. Less internal rotation (**Figure 7**) throughout the propulsion cycle was observed for the Q2. This difference, although noticeable, was not significant. The range of value in orientation angles was, however, remarkably similar in both chairs.

DISCUSSION

There were several differences in temporal parameters between wheelchairs. The changeover from Ppull to Ppush in the Q2 took place nearly 5° behind the position at which this changeover occurred in chair T. This may be due to the axle placement in chair Q2, 2.5 cm forward of the back edge of the seat and thus, equivalently 2.5 cm more forward than the axle of chair T; the Q2 also has a larger wheel diameter. The total PA, however, was not significantly different between chairs, since release occurred about 5° earlier in the Q2,

Table 4.
Comparison of humeral angular positions.

Humeral Angular Displacement	Wheelchair Type Q2 °	Q2 %	T °	T %	Difference °	Difference %	P Value °	P Value %
Plane of Elevation								
at grab	−57.66	—	−57.84	—	0.18	—	0.9165	—
at Δ Ppull to Ppush	−42.36	26.9	−45.03	21.1	2.67	5.8	0.1909	0.0295
at release	−6.10	40.4	9.55	37.5	3.45	2.9	0.4784	0.0998
maximum	27.55	53.6	24.77	50.0	2.78	3.6	0.2184	0.0353
minimum	−59.16	1.9	−59.04	2.3	0.12	0.4	0.9279	0.7239
range	86.71	—	83.81	—	—	—	—	—
Amount of Elevation								
at grab	47.26	—	47.01	—	0.25	—	0.7084	—
at Δ Ppull to Ppush	42.82	26.9	40.80	21.1	2.02	5.8	0.0825	0.0295
at release	31.55	40.4	28.08	37.5	3.47	2.9	0.0014	0.0998
maximum	48.24	6.1	47.50	99.1	0.74	7.0	0.3196	0.0176
minimum	26.59	61.8	23.27	57.8	3.32	4.0	0.0007	0.2617
range	21.65	—	24.23	—	—	—	—	—
Orientation								
at Grab	54.91	—	59.12	—	4.21	—	0.0086	—
at Δ Ppull to Ppush	44.98	26.9	51.95	21.1	6.97	5.8	0.0023	0.0295
at release	21.19	40.4	26.07	32.5	4.88	2.9	0.0113	0.0998
maximum	57.93	8.1	62.75	3.7	4.82	4.4	0.0119	0.0344
minimum	2.06	51.8	6.84	49.0	4.78	2.7	0.0262	0.0333
range	55.87	—	55.91	—	—	—	—	—

° = degrees (absolute displacement); % = percentage of total cycle at which the position was measured at the end of cycle.

offsetting part of the 10° gain in GA. Though not significantly different in magnitude, this difference in PA was gained at an advantageous point in the cycle for chair Q2, primarily during the pull arc, where the elbow flexors can assume a greater role in initiating propulsion. Van der Woude et al. (26) showed a similar shift in cycle landmarks, with the pull phase being cut short as seat height increased (analogous to switching from the Q2 chair to the T chair in this study). Consequently, this lower seat positioning might reduce the burden on the shoulder flexors, shoulder rotators, and scapular stabilizers that would need to be active for propulsion initiated closer to the "twelve o'clock" wheel position. However, this would need to be confirmed with future 3-D kinetic analyses of the shoulder.

In a study of subjects without disabilities who were moderately experienced in wheelchair propulsion, Veeger et al. (40) found that as resistance to propulsion increased, propulsion time also increased. In the current study, subjects consistently reported that they met greater resistance when propelling the Q2. This greater rolling resistance may be due to the width and greater contact area of the Q2 tires with the rollers and the more viscous rubber used for manufacturing the tires. Thus, the slight (but nonsignificant) differences in propulsion times and total cycle times of the two chairs might be in part due to this resistance. Sanderson and Sommer (36) found PPs lasting for 40.5 percent of the total cycle time while the RPs lasted the remaining 59.5 percent of the time. These results are representative of findings in the literature and are remarkably similar to those found in this study (40.4 and 59.6 percent, respectively).

The use of the 1–3′–1″ Euler rotation sequence for describing the motion of the shoulder complex does not translate directly into clinically defined angles for the shoulder. However, this "cyclic" Euler sequence offers several advantages (such as the avoidance of Gimbol lock and the Codman's paradox) over noncyclic Euler sets and projection angle sets commonly used in

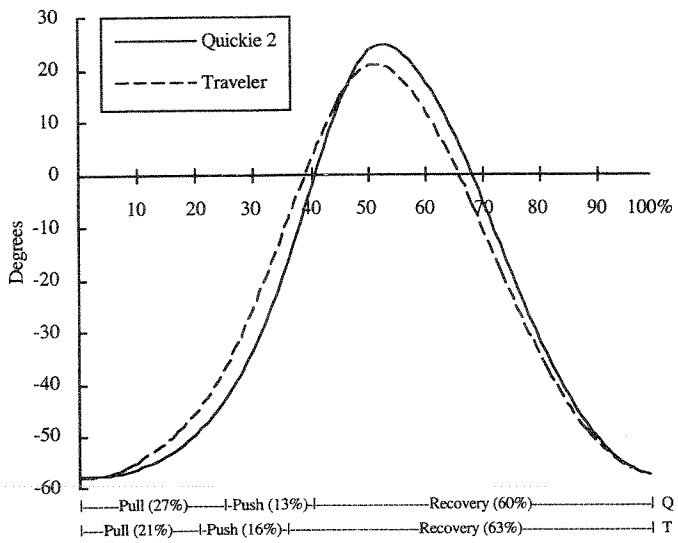

Figure 5.
Mean plane of elevation displacement curves for each wheelchair, all subjects. Positive angle indicates internal rotation of left humerus from the neutral anatomic position. Negative angle indicates external rotation from neutral.

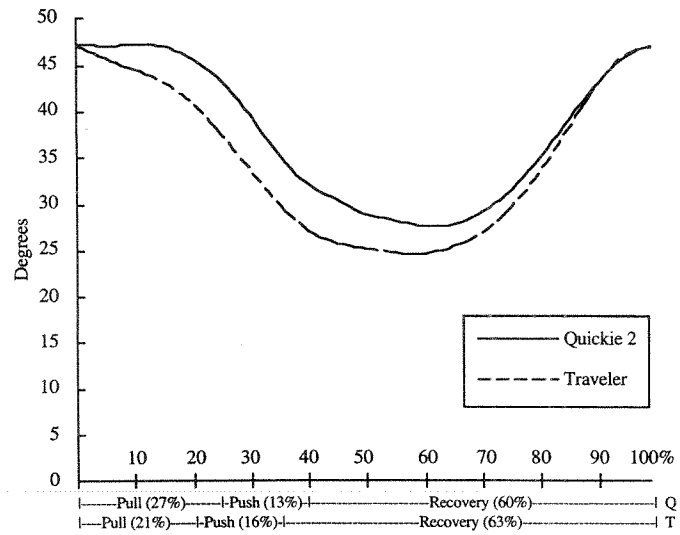

Figure 6.
Mean amount of elevation displacement curves for each wheelchair, all subjects. Positive angle indicates movement of left humerus away from the body.

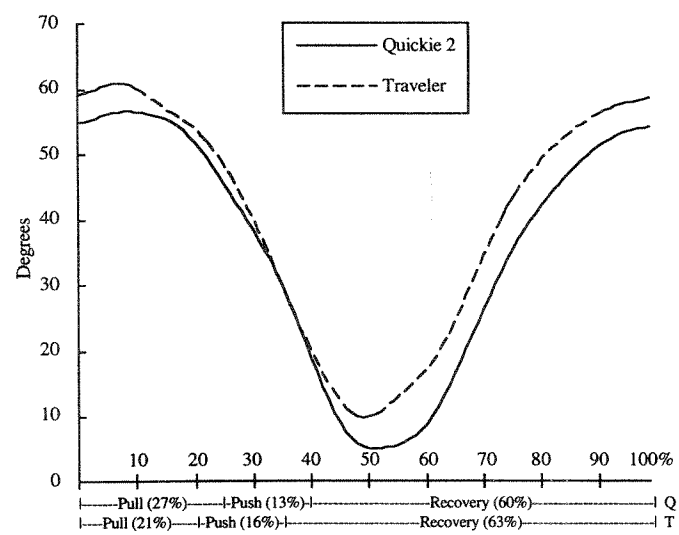

Figure 7.
Mean rotation curves for each wheelchair, all subjects. Positive angle indicates internal rotation of humerus in the final position, negative indicates external rotation.

clinically defined angles by offering a unique description of the humeral posture relative to the trunk (49). Despite the relative inexperience of the subjects of this study, **Figure 4** illustrates that the humeral angle curves are quite reproducible. Though it is not shown graphically, the within-subject, within-trial variability was least during the PP and greatest during the RP. This is suggested to be caused by the fewer degrees of freedom in movement while the hands were in contact with the handrims during propulsion. In this case, the motions were limited by the constraints of a closed kinetic chain system. In contrast, during recovery, the hands may return to the grab position by an almost infinite number of paths (52).

Despite the few statistically significant differences observed at the $p<0.001$ level between any of the angles measured in both chairs, there is room for speculation that a study with a higher statistical power may demonstrate that some significant differences do exist. However, the question remains whether these statistically significant differences (particularly in internal rotation values) would have been clinically significant with magnitudes of about 5°. In lieu of these concerns, an examination of the significant as well as the nonsignificant differences in shoulder angles between the chairs is suggested to be a good demonstration of how these kinematic data may be used to assess the wheelchair propulsion task.

Veeger et al. (40) found that maximal shoulder flexion was reached at the end of the propulsion phase. The amount of flexion reached was dependent on the amount of resistance encountered in turning the handrim. This might explain the trend toward more total

shoulder excursion (plane of elevation and amount of elevation combined) while wheeling the Q2 versus the T chair (**Figures 4** and **5**). The net offset observed in the amount of elevation angle (**Figure 5**) during the entire propulsion cycle in both chairs is suggested to be a necessary mechanism for clearing the arm rests. The smaller angle in chair T during the RP is further suggested to be due to the lower arm rests and the higher and more forward position of the seat relative to the wheel as compared with the Q2.

While there are no comparable data in the literature, the rotation angles measured in this study appear to be within reasonable and expected limits in light of normal ranges of motion for the upper limb. These data were found to follow predictable curves, and extensive testing of the marker set has demonstrated that these data are reproducible. The smaller amount of internal rotation in the Q2 may have been the result of a more upright trunk position subjects assumed in this chair, while the larger internal rotation at grab in chair T may be a result of the greater forward trunk lean of subjects while propelling this chair. Brubaker (53) stated that the fore-aft positioning of the seat relative to the axle in a conventional wheelchair is too far forward for optimal propulsion efficiency. This position forces the user into excessive shoulder internal rotation, extension, and elevation in the recovery phase in preparation for grab. Thus, if the user is positioned more rearward (i.e., more forward axle position as in the Q2 compared with T), the recovery motion is accomplished with considerably less muscular effort to position the arm for grab. Although more internal rotation of the shoulder at grab in chair T was observed, there were no noticeable differences in plane of elevation or amount of elevation angles (which could be considered combinations of shoulder flexion/extension and abduction) observed in this study. Perhaps the advantages of seat position gained by the Q2 for recovery phase shoulder kinematics were offset by the kinematics necessary to clear the higher arm rests, as discussed earlier.

CONCLUSIONS

The 3-D kinematic modeling of the shoulder complex was verified in this study and found appropriate for use in examining activities such as wheelchair propulsion. This project describes only the composite kinematics of the shoulder complex by comparing motions of the humerus with those of the trunk, while recognizing that such motion involves intricate linkages between the humerus, scapula, and thorax. The results of this study could be used in further work isolating individual contributions to absolute humeral excursion for a more detailed description of shoulder motion.

Further, this kinematic model enabled observations of differences in shoulder complex motion as a result of propelling different wheelchair types. This, combined with the observed statistically significant differences in spatio-temporal parameters describing subject-wheel interactions, suggests that differences in design do affect performance. Future studies will hopefully contribute knowledge about whether these differences impact propulsion efficiency or even affect the incidence rate of upper limb injuries.

It appears from the literature that there is a need for more studies of propulsion kinematics using subjects with disabilities who are experienced in wheelchair propulsion. The study by Pentland et al. (2) suggests more work needs to be done in order to understand the possible differences related to gender. The methods established in this study appear to be well suited for many applications, and it is intended that such studies be performed.

REFERENCES

1. Bayley JC, Cochran TP, Sledge CB. The weight bearing shoulder: the impingement syndrome in paraplegics. J Bone Joint Surg 1987;69A:676–8.
2. Pentland WE, Twomey LT. The weight bearing upper extremity in women with long term paraplegia. Paraplegia 1991;29(8):521–30.
3. Gellman H, Chandler DR, Petrasek J, Sie I, Adkins R, Waters RL. Carpal tunnel syndrome in paraplegic patients. J Bone Joint Surg 1988;70A:517–9.
4. Gellman H, Sie I, Water, RL. Late complications of the weight bearing upper extremity in the paraplegic patient. Clin Orthop 1988;233:132–5.
5. Nichols PJR, Norman PA, Ennis JR. Wheelchair user's shoulder. Scand J Rehabil Med 1979;11:27–32.
6. Pennes DR, Shirazi RK, Martel W. Bilateral palmar flexion instability: a complication of wheelchair use. Am J Roentgen 1983;14(6):1327–8.
7. Corcoran PJ, Goldman RF, Hoerner EF, et al. Sports medicine and the physiology of wheelchair marathon racing. Orthop Clin N Am 1980;11(4):697–716.
8. Ferrara MS, Davis RW. Injuries to elite wheelchair athletes. Paraplegia 1990;28:335–41.
9. Brattgard SO, Grimby G, Hook O. Energy expenditure and heart rate in driving a wheelchair ergometer. Scand J Rehabil Med 1970;2:143–8.

10. Cavanagh PR, Kram R. Mechanical and muscular factors affecting the efficiency of human movement. Med Sci Sports Exerc 1985;17(3):326–31.
11. Coutts KD. Dynamic characteristics of a sport wheelchair. J Rehabil Res Dev 1991;28(3):45–50.
12. Davis GM, Shephard RJ. Strength training for wheelchair users. J Sports Med 1990;24-B:25–30.
13. Gass GC, Camp EM. The maximum physiological responses during incremental wheel chair and arm cranking exercise in male paraplegics. Med Sci Sport Exerc 1984;16(4):355–9.
14. Gass GC, Camp EM, Davis HA, Eager D, Grout L. The effects of prolonged exercise on spinally injured subjects. Med Sci Sport Exerc 1981;13(5):277–83.
15. Gayle GW, Pohlman RL, Glaser RM, Davis GM. Cardiorespiratory and perceptual responses to arm crank and wheelchair exercise using various hand-rims in male paraplegics. Res Q Exerc Sport 1990;61(3):224–32.
16. Glaser RM, Sawka JN, Brune MF, Wilde SW. Physiologic responses to maximal effort wheelchair and arm crank ergometry. J Appl Phys 1980;48(6):1060–4.
17. Glaser RM, Sawka MN, Laubach LL, Suryaprasad AG. Metabolic and cardiopulmonary responses to wheelchair and bicycle ergometry. J Appl Phys 1979;46(6):1066–70.
18. Grimby G. On the energy cost of achieving mobility. Scand J Rehabil Med 1983;9:15–9.
19. Harburn L, Spaulding S. Muscle activity in the spinal cord-injured during wheelchair ambulation. Am J Occup Ther 1986;40:629–36.
20. Hilbers PA, White TP. Effects of wheelchair design on metabolic and heart rate responses during propulsion by persons with paraplegia. Phys Ther 1987;67(9):1355–8.
21. Hildebrandt G, Voight ED, Bahn D, Berendes B, Kroger J. Energy costs of propelling a wheelchair at various speeds: cardiac response and effect on steering accuracy. Arch Phys Med Rehabil 1970;51(3):131–6.
22. Martel G, Noreau L, Jobin J. Physiological responses to maximal exercise on an arm cranking and wheelchair ergometer with paraplegics. Paraplegia 1991;29:447–56.
23. Reid M, Lawrie A-T, Hunter J, Warren PM. The effect of steering on the physiological energy cost of wheelchair propulsion. Scand J Rehabil Med 1990;22:139–43.
24. Smith PA, Glaser RM, Petrofsky JS, Underwood PD, Smith GB. Arm crank vs hand rim wheelchair propulsion: metabolic and cardiopulmonary responses. Arch Phys Med Rehabil 1983;64(6):249–54.
25. van der Woude LHV, Veeger HEJ, Rozendal RH, Sargeant AJ. Optimum cycle frequencies in hand-rim wheelchair propulsion. Eur J Appl Physiol 1989;58(6):625–32.
26. van der Woude LHV, Veeger HEJ, Rozendal RH, Sargeant AJ. Seat height in handrim wheelchair propulsion. J Rehabil Res Dev 1989;26(4):31–50.
27. van der Woude LHV, Veeger HEJ, Rozendal RH, et al. Wheelchair racing: effects of rim diameter and speed on physiology and technique. Med Sci Sports Exerc 1988; 20(5):492–500.
28. van der Woude W, de Groot G, Hollander AP, van Ingen Schenau GJ, Rozendal RH. Wheelchair ergonomics and physiological testing of prototypes. Ergonomics 1986; 29:1561–73.
29. van der Woude W, van Ingen Schenau GJ, Rozendal RH, Hollander AP. Manual wheelchair propulsion: effects of power output on physiology and technique. Med Sci Sports Exerc 1988;20(1):70–8.
30. Veeger HEJ, van der Woude LHV, Rozendal RH. Peak oxygen uptake and maximal power output of Olympic wheelchair-dependent athletes. Med Sci Sports Exerc 1991;23(10):49–55.
31. Bardsley G, Rose A. Investigations into the influence of wheel position on the propulsion capabilities of wheelchair users. J Rehabil Res Dev 1991;28(1):454–5.
32. Brown DD, Knowlton RG, Hamill J, Schneider TL, Hetzler RK. Physiological and biomechanical differences between wheelchair-dependent and able-bodied subjects during wheelchair ergometry. Eur J Appl Phys 1990;60(3):179–82.
33. Cerquiglini S, Figura F, Marchetti M, Ricci B. Biomechanics of wheelchair propulsion. In: Morechi A, Fidelin K, Kedzior K, Wit A, editors. Biomechanics VII-A. Baltimore: University Park Press; 1981.
34. Hughes CJ. Biomechanics of wheelchair propulsion as a function of seat position and user-chair interface (dissertation). Charlottesville, VA: University of Virginia; 1990.
35. Masse L, Lamontagne M, O'Riain MD. Biomechanical analysis of wheelchair propulsion for various seating positions. J Rehabil Res Dev 1992;29(3):12–28.
36. Sanderson DJ, Sommer HJ. Kinematic features of wheelchair propulsion. J Biomech 1985;18(6):423–9.
37. van der Woude LHV, Veeger HEJ, Rozendal RH. Propulsion technique in hand-rim wheelchair propulsion. J Med Eng Technol 1989;13:136–41.
38. Veeger HEJ, van der Woude LHV, Rozendal RH. Wheelchair propulsion technique at different speeds. Scand J Rehabil Med 1989;21(4):197–203.
39. Veeger HEJ, van der Woude LHV, Rozendal RH. A computerized wheelchair ergometer: results of a comparison study. Scand J Rehabil Med 1992;24:17–23.
40. Veeger HEJ, van der Woude LHV, Rozendal RH. Within-cycle characteristics of the wheelchair push in sprinting on a wheelchair ergometer. Med Sci Sports Exerc 1991;23(2):264–71.
41. Veeger DHEJ, van der Woude LHV, Rozendal RH. The effect of rear wheel chamber in manual wheelchair propulsion. J Rehabil Res Dev 1990;26(2):37–46.
42. Coutts KD. Kinematics of sport wheelchair propulsion. J Rehabil Res Dev 1990;27(1):21–6.
43. Jarvis S, Rolfe H. The use of an inertial dynamometer to explore the design of children's wheelchairs. Scand J Rehabil Med 1982;14:167–76.
44. Lundberg, A. Wheelchair driving: evaluation of a new training outfit. Scand J Rehabil Med 1980;12(2):67–72.
45. Tupling SJ, Davis GM, Pierrynowski MR, Shephard RJ. Arm strength and impulse generation: initiation of wheelchair movement by the physically disabled. Ergonomics 1986;29(2):303–11.

46. Ruggles D, Cahalan T, An KN. Biomechanics of wheelchair propulsion by able-bodied subjects. Arch Phys Med Rehabil 1994;75:540–4.
47. An KN, Korinek SL, Kilpela T, Edis S. Kinematic and kinetic analysis of push-up exercise. Biomed Sci Instrum 1990;26:53–7.
48. Woltring HJ. A FORTRAN package for generalized cross-validitory spline smoothing and differentiation. Adv Eng Software 1986;8(2):104–13.
49. Morrey BF, An KN. Biomechanics of the shoulder. In: Rockwood CA, Matsen FA, editors. The shoulder. Baltimore: Harcourt Brace Jovanovich, Inc.; 1990. p. 208–44.
50. An KN, Browne O, Korinek S, Tanaka S, Morrey BF. Three dimensional kinematics of glenohumeral elevation. J Orthop Res 1991;9:143–9.
51. Senghas RE. Statistics in the Journal of Bone and Joint Surgery: suggestions for authors. J Bone Joint Surg 1992;74A:319–20.
52. Shephard RJ. Sports medicine and the wheelchair athlete. Sports Med 1988;5(4):226–47.
53. Brubaker C. Choosing a wheelchair system: ergonometric considerations. J Rehabil Res Dev 1990;Clin Suppl 2:37–48.

Submitted for publication April 16, 1996. Accepted in revised form May 20, 1997.